Sustainable Production through Advanced Manufacturing, Intelligent Automation and Work Integrated Learning, J. Andersson et al. (Eds.)

doi:10.3233/ATDE240158

Effect of Laser Power on the Deposition of Alloy 718 Powder on Alumina Substrate Using Laser Directed Energy Deposition: A Single-Track Study

Dilipkumar Choudary RATNALA[a,1] Fabian HANNING[a], Joel ANDERSSON [a], Shrikant JOSHI [a]
[a] *Department of Engineering Science, University West, Trollhättan, Sweden*
ORCiD ID: Dilipkumar Choudary Ratnala https://orcid.org/0000-0002-6605-1869
Fabian Hanning https://orcid.org/0000-0002-1607-9177
Joel Andersson https://orcid.org/0000-0001-9065-0741
Shirkant Joshi https://orcid.org/0000-0001-5521-6894

Abstract. Welding or brazing of metals to ceramics often leads to failures under aggressive conditions due to abrupt changes in physical, chemical, and thermal properties at the metal-ceramic interface. Metal-ceramic Functional Graded Materials (FGMs) replace the strict interface with a gradual transition of composition and properties, which protects the material from failures. The powder-blown Laser-Directed Energy Deposition (DED-LB) is one of the widely known Additive Manufacturing (AM) processes that offer unique features like developing FGMs and multi-material structures. Various studies have been conducted to process metal-ceramic FGMs using the DED-LB process but significant differences in thermal properties, varying laser-material interactions, and the possibility of formation of complex reaction products make the processing of metal-ceramic FGMs challenging. This study aims to understand the effect of laser power on a ceramic substrate, and its interaction with a metal powder introduced in the melt pool. A single track of nickel-based superalloy Alloy 718 powder was deposited on an Alumina substrate with different laser powers. The deposition was performed with and without substrate pre-heat to understand the effect of pre-treatment on deposition. Metallographic analysis was performed to reveal the microstructure of the resolidified metal mixed ceramic region.

Keywords. Laser-Directed Energy Deposition, Metal-Ceramic FGMs, Alumina, Alloy 718

[1] Corresponding Author: Dilipkumar Choudary Ratnala, dilipkumar-choudary.ratnala@hv.se.

1. Introduction

Continuous growth in space exploration, energy production and consumption, and structural engineering requires advanced materials with exceptional properties. In certain circumstances, the application or component demands a specific material with properties like high-temperature strength, low-temperature toughness, high wear, abrasion, ablation, and corrosion resistance, in addition to general mechanical properties[1]. Even though there is constant improvement in the properties of different materials such as metals, ceramics, and polymers, no single material can satisfy all the requirements of the fast-growing aerospace and energy industries. The composite structures developed using dissimilar materials either by joining or other means, manifest improved performance, and diverse application prospects[2].

Ceramics are important engineering materials with good thermal, mechanical, and chemical properties. The usage of ceramics is well-established in areas like aerospace, optics, biomaterials, sensors, body armor, and energy industries. However, brittleness and poor workability restrict the usage of ceramics in producing large-scale components and make their applications limited [1,3]. On the other hand, metals exhibit good thermal and electrical properties, superior ductility with adequate strength, good corrosion resistance, and better processability. Metals are widely used materials in various fields like construction, automobile, petrochemicals, aerospace, and nuclear where weldability, processability, along with manufacturing cost are the key factors. The engineering applications of metals are still limited in certain sectors where high-temperature strength, oxidation resistance, and chemical inertness are crucial. Hence, metal-ceramic joint structures with complementary properties can be a potential solution to overcome the above-stated limitations of each [1,4].

Metal and ceramics are joined either directly by welding or by brazing with the help of suitable filler material [2]. In both cases, a sharp interface exists where the properties of the material change drastically. This sudden variation in properties at the metal-ceramic joint interface leads to uneven stress distribution and ultimately to the failure of the joint. The introduction of an appropriate interlayer, which can alleviate the extreme property mismatch between metals and ceramics, can provide some relief but does not eliminate the interface effect. In this context, the replacement of a sharp interface by a gradual compositional grading of metals and ceramics has the potential to yield a strong metal-ceramic structure with enhanced properties. The materials developed through such a compositional grading strategy are called Functional Graded Materials (FGMs) [2,5].

Manufacturing methods like powder metallurgy, centrifugal casting, and vapor deposition are used to produce FGMs. All the mentioned processes are either time-consuming, or quantity and design-restricted, and require a lot of tooling. Additive Manufacturing (AM) processes like Directed Energy Deposition (DED) and Selective Laser Melting/Sintering (SLM/S) can produce FGMs with minimal tooling. Especially, the powder-based Laser-Directed Energy Deposition (DED-LB) process gives greater flexibility to design complex structures and offers a versatile material selection portfolio [3,5].

The DED-LB process utilizes a high-energy laser beam to create a melt pool on the substrate, into which the powder is directed through a nozzle system. The powder melts and solidifies as the laser beam progresses further. By continuously depositing layer upon layer, a 3D component is produced. The DED-LB system offers the unique advantage of utilizing multiple powder feeders with the capability to independently control the feeding of powder constituents, which can conveniently realize the

production of FGMs. However, there are multiple process parameters that can affect the final deposit microstructure and properties. Laser power, laser spot size, scan speed, hatch spacing, and powder feed rate are some of those parameters that are known to influence the deposition process and final microstructure [1,6,7].

Metal-ceramic FGMs can be produced by the DED-LB process with careful feed rate adjustments from individual metal and ceramic-filled powder feeders. However, the quality of the produced materials mainly depends on the optimal process parameters, and interaction between metals and ceramics in the melt pool [6]. Moreover, the low thermal conductivity and low thermal shock resistance make ceramics sensitive to sudden temperature rise [8,9]. This makes studying the effect of process parameters on FGM deposition and its properties crucial. Out of all the Laser-DED process parameters, laser power, scan speed, and feed rate are considered as dominating. While the scan speed and powder feed rate govern the deposition rate, laser power decides the temperature in the interaction zone and, consequently, influences the melting of the metal-ceramic powders [6,10].

Hence, the objective of this study is to understand the effect of laser power on the geometry and microstructure of the single-track deposited metal powder on the ceramic substrate.

2. Materials and Method

2.1. Materials

Ceramic samples with dimensions of 26 mm diameter and 6 mm thickness were used as substrates. These substrates were composed of 96% Al_2O_3 and 4% SiO_2 + CaO. Gas-atomized Alloy 718 powder manufactured by Höganäs AB, Sweden was deposited on the ceramic substrate. The nominal chemical composition of the feedstock powder is reported in Table 1. The metal powder has a particle size range of 45-90 µm with spherical morphology. The powder has, however, been sieved to 75µm to avoid possible feeding problems with the used powder nozzle. The particle size distribution and presence of the satellites on powder particles can be observed in Figure 1.

Table 1. Nominal chemical composition, in wt%, of Alloy 718 metal powder.

Element	Ni	Cr	Nb	Mo	Ti	Al	Minor elements	Fe
Composition (wt%)	50-55	17-21	4.75-5.50	2.8-3.3	0.6-1.2	0.2-0.8	2-2.5	Balance

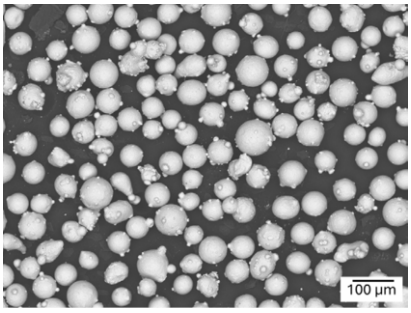

Figure 1. Morphology and particle size distribution of Alloy 718 metal powder.

2.2. Experimental Method

A Trumpf Trudisc 12002 laser system with a 12kW laser source and a Fraunhofer coaxial continuous powder nozzle with annular outlets were used to deposit Alloy 718 powder on the Alumina substrate. A volumetric powder feeder with pure Argon as carrier gas (volumetric flow rate of 8 l/min) was used to deliver powder into the interaction zone of the DED-LB system. Additionally, Argon with a flow rate of 10 l/min was also used as a shielding gas to shield the melt pool. A hot plate with resistance heating was used to preheat the substrates to 400-450 °C. The single-track deposition experiments were performed using a laser optical fiber of 0.4 mm diameter and with process parameters provided in Table 2. Laser scan speed and powder feed rate were fixed throughout the experiments[11], and the laser power varied from 1200 W to 600 W. The experiments were performed with and without substrate preheating to understand the effect of preheating on deposition.

Table 2. Laser process parameters used for single-track experiments.

Power (W)	Scan speed (mm/s)	Powder feed rate (g/min)	Scanning strategy	Deposition length (mm)
1200, 1000, 800, 600	12	13	Single bead	20

2.3. Characterization

The ceramic substrates with single-track deposits were prepared for metallographic analysis. Cross-sections perpendicular to the deposition direction were prepared using a Buehler IsoMet4000 precision cutting machine. Samples were mounted, grinded, and then polished using 9 µm, 6 µm, and 3 µm diamond suspensions to reveal geometrical and microstructural features. Light Optical Microscopy (LOM) of the prepared samples was conducted using Zeiss Axio Imager M2m coupled with Zeiss ZEN2 Core software. For microstructural and compositional analysis, a Zeiss Gemini Field Emission Scanning Electron Microscope (FE-SEM) connected to Oxford AZtec Energy Dispersive X-ray Spectroscopy (EDS) was used.

Hardness measurements were performed with a Vickers microhardness indentation test using a Struers Duramin 40 micro and macro hardness testing machine. The indents were evenly distributed over the bead cross-section with a 200 g load and a dwell time of 10 s [10].

3. Results

3.1. As deposited samples´ condition

The condition of the deposited samples is shown in Figure 2. Metal powder deposition performed on Alumina substrates without preheating resulted in cracks for all the conditions. The cracked samples were impossible to cut and process further. The deposition on preheated Alumina substrates resulted in a single-track deposition as shown in Figure 2c.

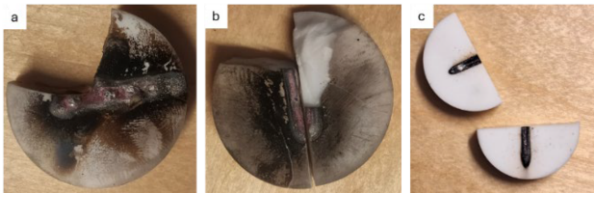

Figure 2. As deposited samples: a and b- without substrate preheating, c- with preheating (samples after cutting).

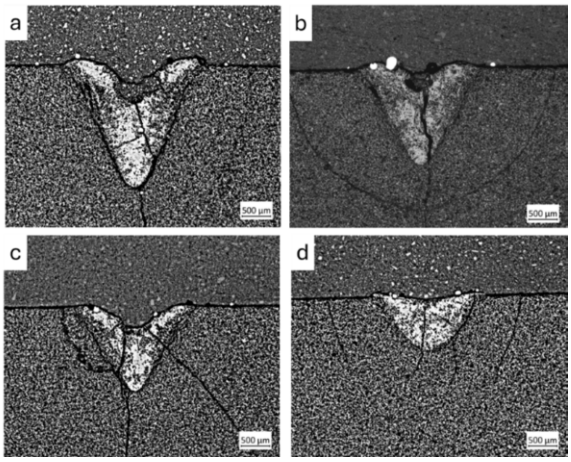

Figure 3. Optical micrographs of single-track deposits on preheated alumina substrate at different laser power conditions: a-1200 W, b-1000 W, c-800 W, d-600 W.

3.2. Geometrical features of deposits

The light optical microstructure images of transverse cross-sectioned single-track deposits are shown in Figure. 3. It is evident from the microstructures that, with variation in laser power, there is a significant difference in the geometry of the deposited bead. The microstructures of all the samples illustrate improper deposition which is unlike the geometry of a typical DED-LB deposit (Figure 4). With a decrease in laser power from 1200 W to 600 W, there is a constant change in track geometry. The measured dimensions of the width and depth of depositions are provided in Figure. 5. The width of the track varied between 2.2 mm to 1.8 mm for different laser power conditions (from 1200 W to 600 W). The depth varied from 2.06 mm for the high laser power of 1200 W to 0.86 mm for the low laser power setting of 600 W. It can be observed that, with variation in laser power from high to low, the depth of the deposition was affected more than the height. There are observable cracks in all the samples processed using different laser powers. All cracks are longitudinal in nature and almost start at the center of the track where the terminal solidification occurs during the deposition process. It can also be observed in Figures 3a,3b, and 3c that cracks started at the center and penetrated all through the substrate but in the deposition performed with low laser power (Figure 3d), cracks are restricted only to some parts of the substrate. This demonstrates the effect of laser power on the cracks in the deposition.

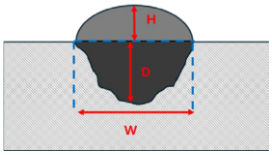

Figure 4. Illustration of a typical single-track bead geometry of Laser Directed Energy Deposited (DED-LB) sample showing H- height, D- depth, and W- width.

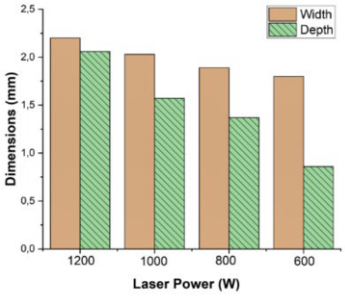

Figure 5. Geometrical dimensions (width and depth) of deposits at different laser power conditions.

3.3. Microstructural analysis of deposits

From the high magnification microstructures provided in Figure 6, traces of some un-melted or semi-molten powder particles in the deposited region can be observed. This might be due to a lack of optimal process parameters. The microstructure has three different regions: A continuous grey phase with distinct grains growing on the substrate towards the surface, a distributed dark phase, and bright resolidified particles that are in the nanoparticle range. A similar microstructure is observed in all the samples deposited at various laser power conditions as shown in Figure 7. The interface between the solidified region and substrate illustrates the epitaxial growth of grains in the deposited region. From Figure 8a it is clear that resolidified particles are aligned along the grain boundaries and also inside the elongated grains, which represent these particles as a product of metal-ceramic solidification. These resolidified particles are well-distributed along the bead for all the deposition conditions, which demonstrates a properly mixed melt pool for all the laser powers used.

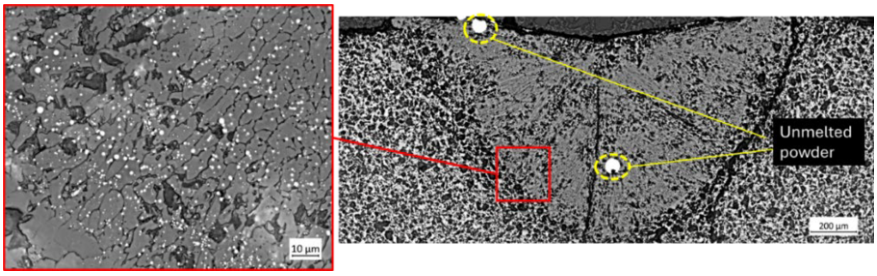

Figure 6. Optical micrograph showing the presence of unmelted Alloy 718 powder and resolidified particles in the deposited area.

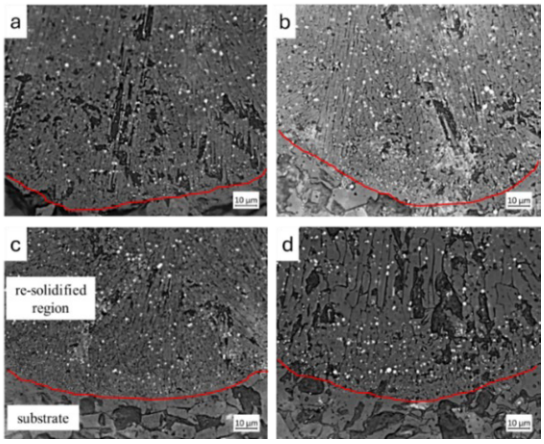

Figure 7. Cross-sectional optical micrographs at higher magnification with grain growth of samples deposited at different laser power conditions. a-1200 W, b-1000 W, c-800 W, d-600 W

EDS area mapping as shown in Figure 8 confirms the chemical composition of different regions in the microstructure. The continuously growing grains are of Aluminum oxide whereas distributed patched regions are of Silicon oxide. The presence of Silicon can be ascribed to the substrate composition. Point analysis of bright particles reveals that Cr, Fe, Ni, and Nb are the major constituents (shown in Figure 9b). This can be related to the saturation capacities of these elements in the Alumina melt (explained in the discussion section). The observed particles are in different size ranges but have almost similar compositions.

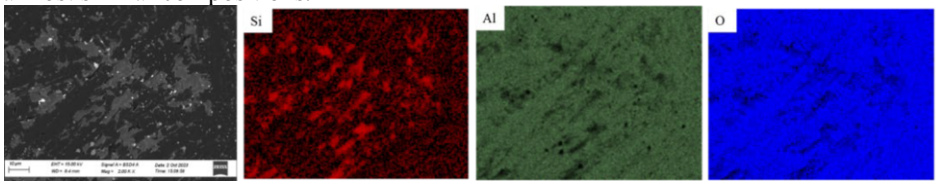

Figure 8. Electron Dispersive X-ray Spectroscopy (EDS) area map showing the presence of Aluminum oxide (dark region) and Silicon oxide (grey region) in the deposit.

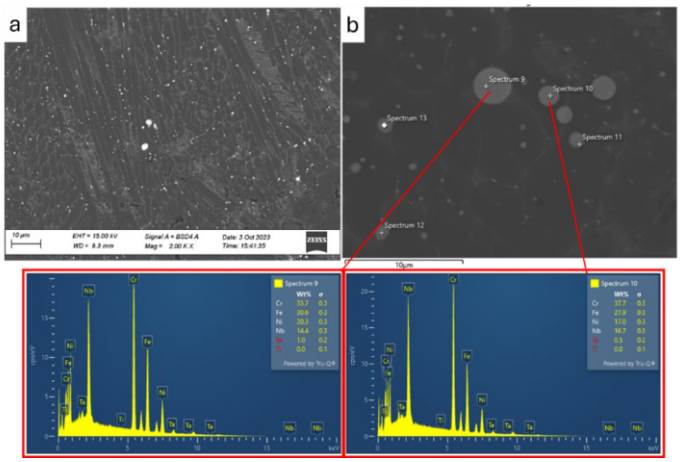

Figure 9. a) Microstructure with bright particles distributed in the deposited region, b) Electron Dispersive X-ray Spectroscopy (EDS) point analysis of these bright resolidified particles.

3.4. Microhardness

Vickers micro-indentation hardness data is provided in Figure 10. The highest hardness value is 1825 $HV_{0.2}$, while the lowest hardness value is 1653 $HV_{0.2}$. With a decrease in laser power, there is a significant increase in hardness levels. The microhardness of the substrate is only 1058 $HV_{0.2}$, which demonstrates that laser power has a significant effect on improving the microhardness of the sample, due to the rapid solidification that happened during the deposition. The obtained microhardness values are on par with the values obtained by Youzhou Li et al. who used Laser Engineered Net Shaping (LENS) for alumina ceramic processing [7].

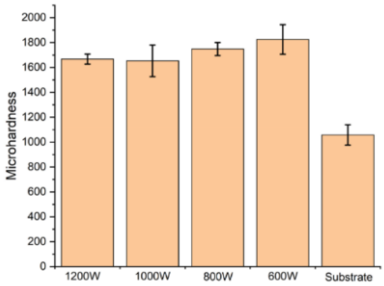

Figure 10. Vickers microhardness of samples deposited with different laser power conditions and the unaffected substrate.

4. Discussion

4.1. Effect of substrate pre-heating on deposition

The Alumina substrates used for deposition without any preheating were not able to withstand the stresses generated during the deposition. As the thermal conductivity and thermal shock resistance of alumina ceramic is low, it tends to crack when exposed to sudden temperature rise. During the laser deposition process, an intense amount of heat is concentrated on a very small area of the Alumina substrate. Ineffective heat conduction to the substrate along with low resistance to thermal shock, made the samples crack sensitive. The Alumina samples deposited with preheating of 400-450 °C, also resulted in cracks but those cracks were not so intense to completely damage the sample (as can be observed in Figures 2 and 3). The preheating of the substrate decreased the difference in temperature attained during the deposition and allowed the substrate to accommodate the stresses generated due to heat conduction.

4.2. Deposit geometry

The understanding of the cross-section geometry of the single-track deposits is important as it provides useful insights into the effect of process parameters on the substrate. The metallurgical bonding between the substrate and deposited region along with the height, depth, and width of the deposition plays a significant role in assessing the productivity of the used process parameters. For a laser beam of fixed diameter, the

energy density (intensity of energy per unit area) depends mainly on laser power and scan speed. As in these experiments scan speed is kept constant, laser power had a great contribution in deciding the geometry of the deposit. It can be observed that, with the decrease in laser power from 1200 W to 600 W, there is a continuous change in the geometry of the track. Figure 5 demonstrates that depth is more affected than width by power, as high laser power imposes high energy density on the substrate.

4.3. Deposit Microstructure

Optical microstructures of the single-track deposits show longitudinal cracks in samples deposited with all the laser power conditions. All these cracks originate from the center of the deposit where terminal solidification takes place. According to Y. Zheng et al., rapid solidification of alumina leads to longitudinal cracks which are partly generated from solidification and by deflection of transverse cracks [12]. These longitudinal cracks are mainly caused due to high-temperature gradients and by the internal stresses developed in the samples due to the low thermal shock resistance [12]. During the deposition process, solidification of the melt starts from the boundary of the melt pool and proceeds towards the center, while solidification shrinkage proceeds from the center of the melt pool to the boundary. This opposite action of solidification shrinkage generates tensile stresses towards the boundary which forms longitudinal cracks at the center of the deposit [12]. With an increase in laser power, there is an increase in temperature gradient which causes heat dissipation at a faster rate and, consequently the solidification rate [12]. In the single-track experiment performed, with the increase in laser power, there is an observable increase in crack intensity from the center of the track to the substrate. For deposition performed at 600 W, crack intensity is less, which can be ascribed to lower tensile stresses resulting from the reduced temperature gradient.

The bead microstructures observed in cross-sections demonstrated three distinct phases or regions in the track. From EDS analysis (Figures 8 and 9) it can be observed that alumina is a matrix with silicon oxide and a well-distributed metallic phase composed of Cr, Ni, Fe, and Nb as small particles. Though the composition of the particles is like that of the Alloy 718 feedstock powder, the size of the particles is in nanometer size and not in the range of feedstock particle size distribution. It suggests that these particles are the products of solidification. In the melt pool, when all the constituents are in the molten state, chemical reactions between individual constituents lead to different products[1,4]. For the given single-track deposition, Aluminum as the major constituent dominates the phase fraction. When constituents like Ni, Cr, and Fe enter the melt pool via the added Alloy 718 powder, the solubility of these elements in Al dictates the final chemical products. The maximum solubilities of Ni, Cr, and Fe in Al are 0.04 wt%, 0.7 wt%, and 0.05 wt% respectively at 650 °C where the solidification of Al starts [13]. Due to this extremely low solubility, metallic elements tend to segregate out of the Al matrix during solidification. In addition, Al has a higher affinity towards oxygen to form oxides by virtue of its low Gibbs free energy of the oxide formation. According to S.C. Kuiry et al., if the contact angle between the metal and ceramic is high, then the molten metal tends to transform into nano-spherical particles inside the ceramic during laser processing [14]. It was reported that the contact angle between liquid Ni and Alumina is approximately 110°, which leads to the formation of spherical Ni nanoparticles in the Alumina matrix during rapid solidification [14]. It suggests that the segregation of metallic content as separate particles in the deposit is due to low solubility

and wettability. The presence of metallic particles can be seen in all the samples irrespective of laser power conditions.

4.4. Microhardness

The microhardness of the deposit is influenced by various factors like grain size, chemical composition, and stress conditions. In comparison to the hardness of the substrate, samples deposited using different power conditions exhibited higher hardness. It is common to attain a fine grain size during rapid solidification, which shows a considerable impact on hardness. As the grain size of the deposited region is fine, improvement in hardness is observed for all samples. With an increase in laser power, there is a slight decrease in hardness which remains constant above 1000 W without significant variation. This suggests that laser power has more effect on microhardness at low power levels than at high power levels. As metallic content is present in all the specimens, its effect on hardness is not clear and requires further analysis.

5. Conclusions

The present single-track deposition study investigated the effect of one of the laser process parameters, laser power, on the geometry and microstructure of Alloy 718 powder deposited on an Alumina substrate. It also evaluated the effect of substrate preheating on deposition.

1. The samples deposited without preheating led to intense cracks and made further analysis difficult. Preheated ceramic substrates resisted the thermal stresses generated during the deposition process as preheating decreased the temperature gradient.
2. Laser power showed considerable effect in determining the deposited sample´s geometry and crack sensitivity. With a decrease in laser power, a continuous change in geometry and decreased crack tendency can be observed. As laser scan speed also shows a considerable effect on the geometry of the deposit, optimizing the parameters is necessary to avoid cracks even at low laser powers.
3. Laser power did not show any direct influence on the microstructural features, as all the samples consisted of the same phases (Alumina, Silicon oxide, and metallic phase). The low solubility of metallic elements (Ni, Fe, and Cr) in the ceramic phase led to the formation of small spherical particles in the deposit. The effect of these particles on the microhardness of the samples is not yet clearly understood. However, deposition with low laser powers showed an increase in the hardness of the sample in the deposited region.

References

[1] Y. Hu, W. Cong, A review on laser deposition-additive manufacturing of ceramics and ceramic reinforced metal matrix composites, Ceram Int. 44 (2018) 20599–20612. https://doi.org/10.1016/j.ceramint.2018.08.083.

[2] Y. Zhang, Y.K. Chen, D.S. Yu, D.Q. Sun, H.M. Li, A review paper on effect of the welding process of ceramics and metals, Journal of Materials Research and Technology. 9 (2020) 16214–16236. https://doi.org/10.1016/j.jmrt.2020.11.088.

[3] W. Zheng, D. Zhang, D. Wu, N. Ma, P. Geng, Effects of ceramic material in laser-directed energy deposition of titanium/ceramic functionally graded materials, J Mater Process Technol. 317 (2023). https://doi.org/10.1016/j.jmatprotec.2023.117992.

[4] M.A. Mahmood, A.C. Popescu, I.N. Mihailescu, Metal matrix composites synthesized by laser-melting deposition: A review, Materials. 13 (2020). https://doi.org/10.3390/ma13112593.

[5] B. Saleh, J. Jiang, R. Fathi, T. Al-hababi, Q. Xu, L. Wang, D. Song, A. Ma, 30 Years of functionally graded materials: An overview of manufacturing methods, Applications and Future Challenges, Compos B Eng. 201 (2020). https://doi.org/10.1016/j.compositesb.2020.108376.

[6] D. Svetlizky, M. Das, B. Zheng, A.L. Vyatskikh, S. Bose, A. Bandyopadhyay, J.M. Schoenung, E.J. Lavernia, N. Eliaz, Directed energy deposition (DED) additive manufacturing: Physical characteristics, defects, challenges and applications, Materials Today. 49 (2021) 271–295. https://doi.org/10.1016/j.mattod.2021.03.020.

[7] Y. Li, Y. Hu, W. Cong, L. Zhi, Z. Guo, Additive manufacturing of alumina using laser engineered net shaping: Effects of deposition variables, Ceram Int. 43 (2017) 7768–7775. https://doi.org/10.1016/j.ceramint.2017.03.085.

[8] F. Niu, S. Yan, G. Ma, D. Wu, Directed-Energy Deposition for Ceramic Additive Manufacturing, in: Additive Manufacturing Processes, ASM International, 2020: pp. 131–151. https://doi.org/10.31399/asm.hb.v24.a0006559.

[9] J. Odinot, A. Julian-Jankowiak, J. Petit, D. Choron, D. Boisselier, M. Thomas, Direct laser additive manufacturing of ceramics by powder deposition, in: Materials Science Forum, Trans Tech Publications Ltd, 2018: pp. 2178–2183. https://doi.org/10.4028/www.scientific.net/MSF.941.2178.

[10] Y. Li, Y. Hu, W. Cong, L. Zhi, Z. Guo, Additive manufacturing of alumina using laser engineered net shaping: Effects of deposition variables, Ceram Int. 43 (2017) 7768–7775. https://doi.org/10.1016/j.ceramint.2017.03.085.

[11] S. Sreekanth, K. Hurtig, S. Joshi, J. Andersson, Influence of laser-directed energy deposition process parameters and thermal post-treatments on Nb-rich secondary phases in single-track Alloy 718 specimens, J Laser Appl. 33 (2021). https://doi.org/10.2351/7.0000259.

[12] Y. Zheng, K. Zhang, T.T. Liu, W.H. Liao, C.D. Zhang, H. Shao, Cracks of alumina ceramics by selective laser melting, Ceram Int. 45 (2019) 175–184. https://doi.org/10.1016/j.ceramint.2018.09.149.

[13] F. Yin, C. Wu, Z. Li, M. Zhao, Y. Liu, Phase equilibrium of the Fe-Cr-Ni-Al quaternary system at 900°C, J Phase Equilibria Diffus. 34 (2013) 181–187. https://doi.org/10.1007/s11669-013-0232-3.

[14] S.C. Kuiry, S. Wannaparhun, N.B. Dahotre, S. Seal, In-situ formation of Ni-alumina nanocomposite during laser processing, Scr Mater. 50 (2004) 1237–1240. https://doi.org/10.1016/j.scriptamat.2004.02.005.